Chapter 31

Mathematics of Experimentally Generated Chemoattractant Gradients

Marten Postma and Peter J.M. van Haastert

Summary

Many eukaryotic cells move in the direction of a chemical gradient. Several assays have been developed to measure this chemotactic response, but no complete mathematical models of the spatial and temporal gradients are available to describe the fundamental principles of chemotaxis. Here we provide analytical solutions for the gradients formed by release of chemoattractant from a point source by passive diffusion or forced flow (micropipettes) and gradients formed by laminar diffusion in a Zigmond chamber. The results show that gradients delivered with a micropipette are formed nearly instantaneous, are very steep close to the pipette, and have a steepness that is strongly dependent on the distance from the pipette. In contrast, gradients in a Zigmond chamber are formed more slowly, are nearly independent of the distance from the source, and resemble the temporal and spatial properties of the natural cAMP wave that *Dictyostelium* cells experience during cell aggregation.

Key words: Diffusion, Equation, Chemotaxis, *Dictyostelium*, Point source, Pipette, Zigmond chamber

1. Introduction

Chemotaxis is a vital process in a wide variety of organisms, ranging from bacteria to vertebrates. Prokaryotes use chemotaxis to move toward high nutrient concentrations or away from unfavorable conditions, while in eukaryotes it is also involved in embryogenesis, wound healing and the immune response. Chemotaxis is achieved by coupling gradient sensing to basic cell movement. Prokaryotes are too small to sense spatial gradients and therefore rely on temporal changes of the chemoattractant concentration to achieve chemotaxis. They do this by adjusting their tumbling frequency in response to temporal changes of the chemoattractant concentration *(1)*. Eukaryotic cells are typically

Tian Jin and Dale Hereld (eds.), *Chemotaxis,* Methods in Molecular Biology, vol. 571
DOI 10.1007/978-1-60761-198-1_31, © Humana Press, a part of Springer Science+Business Media, LLC 2009

large enough to be able to measure a spatial gradient. The difference in receptor occupation between each side of the cell leads to an internal polarization. A pseudopod is extended at the side with the highest receptor occupation and at the same time, pseudopod formation at all other sides is repressed, resulting in directional cell migration *(2, 3)*.

Dictyostelium is a eukaryotic organism that is widely used to study chemotaxis *(4–6)*. Starved *Dictyostelium* cells periodically secrete cAMP. Through relay of the cAMP signal by neighboring cells, concentric cAMP waves are generated. Starved *Dictyostelium* cells are chemotactically sensitive to cAMP and by movement in the direction of the origin of the cAMP waves the cells are able to aggregate into groups of up to 1,000,000 cells. The chemotactic response of *Dictyostelium* is optimized for the dynamic cAMP waves that coordinate both aggregation and multicellular development. Cells show a much stronger chemotactic response to a cAMP wave where the mean concentration increases over time, than to a static spatial gradient. *Dictyostelium* uses both spatial gradient sensing and the "bacterial-like" temporal gradient sensing to respond to these dynamic chemoattractant gradients *(7–9)*.

Several chemotaxis assays have been developed that can be divided into two groups, depending on how the gradient developed. In Zigmond chambers, cells are placed on a bridge separated by a chemoattractant source and a sink reservoir *(10)*. A gradient will be formed under the bridge, which will be nearly linear when at equilibrium. Depending on the geometry of the bridge (which in most setups is a few mm) half-maximal equilibrium is reached only after several minutes. Dunce chambers have similar properties: a linear gradient that is formed during several minutes of incubation.

Many experiments are performed with micropipettes, because this allows the precise positional stimulation of the cell *(11)*. Since the pipette is usually in the field of microscopic observation, distances are relatively small (less than 200 μm) and equilibrium is established very fast on the order of seconds. Since a micropipette behaves like a point source, the gradient will be nonlinear approaching the equation $dC/dx = \nabla C = 1/x^2$ where x is the distance from the pipette. Thus, close to the pipette, the gradient is very steep (~100% per cell of 10 μm length at a distance of 10 μm from the pipette) while more shallow at the edge of the field of observation (10% per cell at a distance of 100 μm). In this manuscript we derive mathematical equations for the temporal and spatial properties of the gradients formed in a Zigmond chamber and delivered from a pipette. We compare the theoretical properties of these gradients with experimental data measuring the gradients using fluorescent dyes. Finally we compare these experimental gradients with those observed during the natural aggregation of *Dictyostelium* cells.

2. Zigmond Chamber-Generated Gradients

2.1. Experimental Setup for Zigmond Chamber

Figure 1a shows the experimental setup with our modified Zigmond chamber *(10)*. On a microscope slide, a glass bridge of ~2 mm wide and 24 mm long was placed on top of two supporting glass strips with thickness 0.15 mm. Cells were placed under the bridge to yield a density of 3×10^4 cells/cm^2. A block of agar containing only buffer was placed at one side of the bridge, while a block of agar containing cAMP and buffer was placed at the other side, which induces the formation of a cAMP gradient under the bridge. Cells were observed by phase contrast microscopy in an area of 350 × 270 μm or by confocal fluorescence microscopy in an area of 150 × 150 μm, both at a distance of 600–700 μm from the agar block containing cAMP.

2.2. Measurement/ Analysis for Zigmond Chamber

The formation of the cAMP gradient was deduced by measuring the diffusion across the bridge of the modified Zigmond chamber using bromophenol blue (Mw = 670 Da). This reveals that a gradient developed during the first few minutes after the cAMP containing agar block was placed against the bridge **(Fig. 1b)**. A stable linear spatial gradient was reached at 5–10 min. This spatial gradient remained approximately constant for 30 min, and then slowly diminished due to depletion of the cAMP source and accumulation of cAMP in the buffer sink **(Fig. 1c)**. Thus the gradients in the modified Zigmond chamber have temporal and spatial components during the first 5 min, but stable spatial gradients during the subsequent 30 min of the experiment.

2.3. Diffusion Equations for Zigmond Chamber

When a large reservoir with cAMP is connected to another large empty reservoir through a thin bridge, diffusion will occur that can be modeled essentially with a one-dimensional diffusion equation in Cartesian coordinates:

$$\frac{\partial C(x,t)}{\partial t} = D\frac{\partial^2}{\partial x^2}C(x,t) \qquad (1)$$

In this equation D (μm^2/s) denotes the diffusion coefficient of cAMP, $C(x,t)$ denotes the concentration at time t (s) and position x (μm) from the source. This equation is solved with the following boundary conditions: the concentration at $x = 0$ (source) is constant with value C_s, the concentration at $x = L$ (sink) is

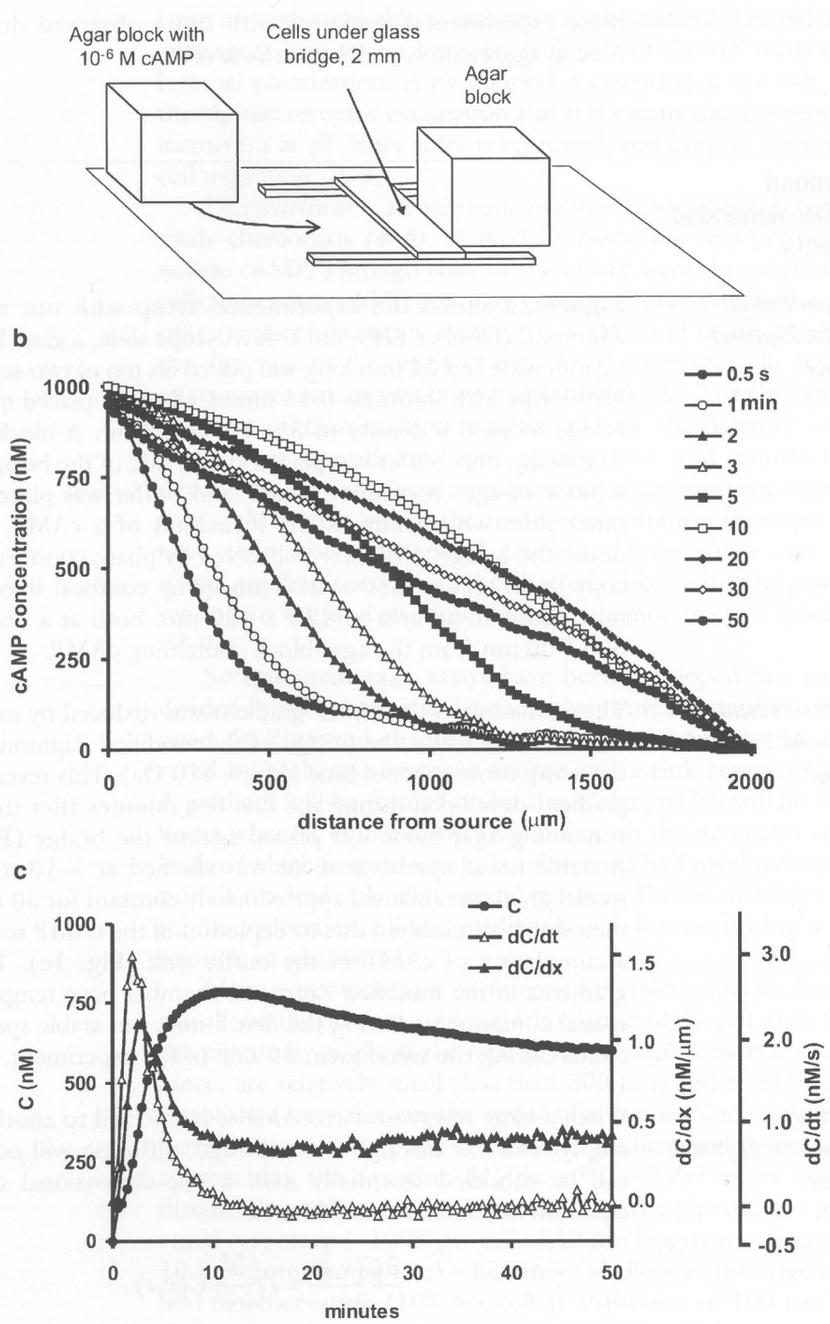

Fig. 1. Observed gradients in the modified Zigmond chamber. (**a**) Setup of the Zigmond chamber. A glass bridge of ~2 mm wide and 24 mm long was placed on top of two supporting glass strips with thickness 0.15 mm. Cells were placed under the bridge. A block of agar containing only buffer was placed at one side of the bridge, while a block of agar containing 1 μM cAMP and buffer was placed at the other side. (**b**) A gradient of cAMP develops under the bridge, visualized by diffusion of a dye added to the agar block containing cAMP. (**c**), gradients at the position of chemotactic observation (650–750 μm from the source). Using the local concentration of the dye we calculated the cAMP concentration C, the spatial gradient d*C*/d*x*, and temporal cAMP gradient d*C*/d*t*.

assumed to be constant and zero. L is the length of the bridge. The complete space-time solution of the concentration profile is then given by:

$$C(x,t) = C_s\left(1-\frac{x}{L}\right) - C_s\sum_{n=1}^{\infty} 2a_n^{-1}\sin\left(a_n\frac{x}{L}\right)e^{-\frac{t}{\tau_n}} \qquad (2)$$

where $a_n = \pi n$, the time constants $\tau_n = a_n^{-2}\tau_D$ and $\tau_D = L^2/D$. The slowest time constant is τ_D/π^2.

After some time equilibrium will appear with a time constant $\tau_D = L^2/D$. The equilibrium concentration profile is given by the first term of **Eq. 2**:

$$C(x) = C_s\left(1-\frac{x}{L}\right) \qquad (3)$$

The gradient and the relative gradient are then given by:

$$\nabla C(x) = -\frac{C_s}{L} \qquad (4)$$

and

$$\frac{\nabla C(x)}{C(x)} = -\frac{1}{L-x} \qquad (5)$$

Figure2 reveals that cAMP will diffuse from the source block approaching a steady state after about 10–20 min. The spatial gradient is initially very steep close to the source block and very shallow at the sink block **(Fig. 2b)**. Over time the gradient decreases in the half of the chamber closest to the source, but increases at the other half closest to the sink. Finally a steady state is reached at 10–20 min, with a magnitude that depends on the cAMP concentration in the source and the width of the bridge. With $C_s = 1$ μM cAMP as source and a bridge of $L = 2{,}000$ μm, the steady-state spatial gradient is constant at $\nabla C = 5$ nM/μm. In the field of observation (600–700 μm from source) the absolute concentration C changes from 700 to 650 nM, and the relative spatial gradient from 0.77 to 0.83% across the cell. The temporal gradient profile is presented in **Fig. 2c**, showing that it reaches a maximum with magnitude and at a time that depends on the distance from the source. Close to the source the maximal temporal gradient is very high and early, and becomes lower and later further away from the source.

The experimental data of bromophenol blue diffusion **(Fig. 1b)** are in close agreement with the model, except for very long incubation times. Since the source and the sink are not indefinitely large, the concentrations in the source and sink slowly decrease and increase, respectively. As a consequence, the gradient will slowly collapse **(Fig. 1c)**. At the position where the cells are observed

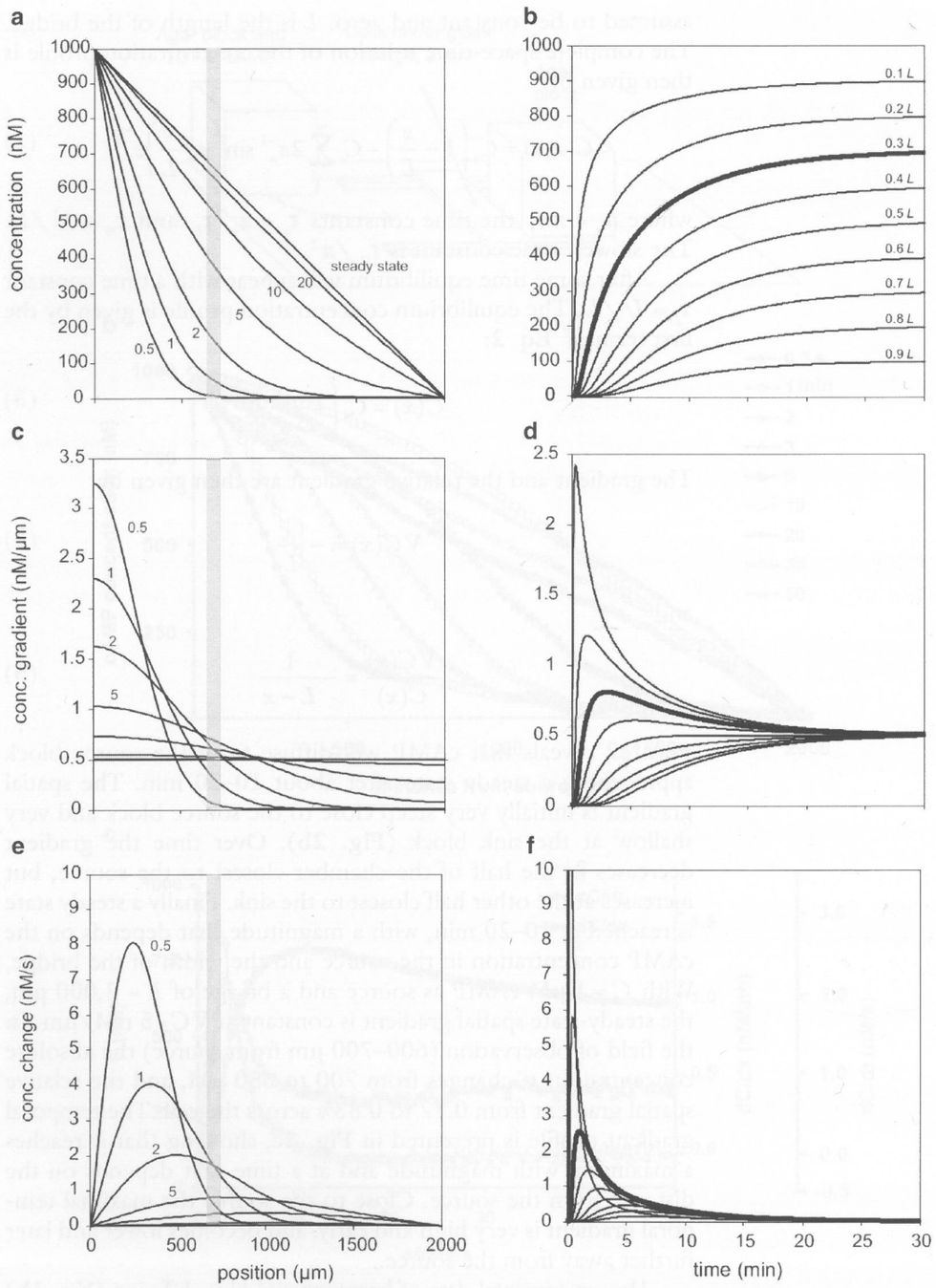

Fig. 2. Theoretical data for Zigmond chamber. **Equation 2** was used to calculate the concentration dynamics. Panels (**a**, **d**) present the concentration C. The spatial gradient d*C*/d*x* is presented in panels (**b**, **e**) and the temporal gradient d*C*/d*t* in panels (**c**, **f**), all at different positions and times from the source containing 1 µM of cAMP. The *gray bars* in the *left panels* and the *thick line* in the *right panels* indicate the place of chemotactic observation (650–750 µm from the source).

using the microscope (600–700 µm from the source), this becomes significant only after more than 2 h, much longer than the 30 min to perform the experiments. Closer to the source or the sink the gradient deviates from a linear gradient sooner **(Fig. 1b)**. At short incubation times, the gradient is formed from 10 to 90% of the equilibrium value in about 4 min, which is only slightly slower than the formation of the cAMP wave during *Dictyostelium* cell aggregation (*see* later). The model and experimental data imply that the modified Zigmond chamber allows two assay conditions: during the first 5 min, the gradient is formed and therefore cells are exposed to both temporal and spatial gradients. The magnitude of these gradients resembles the temporal and spatial gradient of the natural cAMP wave during *Dictyostelium* chemotaxis (*see* **Fig. 5** and Subheading 4). After 10 min a stable gradient is formed without a temporal component.

3. Micropipette-Generated Gradients

3.1. Experimental Setup for Pipette Assay

For the micropipette assay, a droplet of a cell suspension was placed on a glass slide yielding a cell density of 5×10^4 cells/cm^2; the droplet has a diameter of about 10 mm and a height of 3 mm. After the cells were allowed to adhere, a pipette filled with 100 µM cAMP is placed just above the glass surface. cAMP was delivered from the femtotip at a pressure ranging from 0 to 100 hPa.

3.2. Measurement/ Analysis for Pipette Assay with and Without Flow

The formation of the cAMP gradient was deduced by measuring the diffusion of the fluorescent dye lucifer yellow (Mw = 457 Da) using confocal microscopy. The fluorescence intensity at different distances from the pipette was recorded in pixel elements (0.404 × 0.404 µm) using excitation at 488 nm and a 520–550 nm band pass filter for the emission. The data were calibrated using the fluorescence intensity of diluted lucifer yellow added homogeneously to the bath **(Fig. 3a)**. The deduced cAMP concentration profile **(Fig. 3b)** reveals a steep gradient in the vicinity of the pipette that rapidly declines at longer distances from the pipette. This gradient was stable within 20 s after application of the pipette. The concentration at the tip of the pipette is only 150 nM, compared to the 100 µM cAMP inside the pipette.

The amount of cAMP released from the pipette can be increased by applying pressure to the pipette, which induces a steady flow of cAMP that diffuses away. The cAMP concentration profile was again deduced from the pipette containing lucifer yellow, revealing that the concentration at the tip increases from 150 nM cAMP without pressure to 3,000 nM cAMP at a

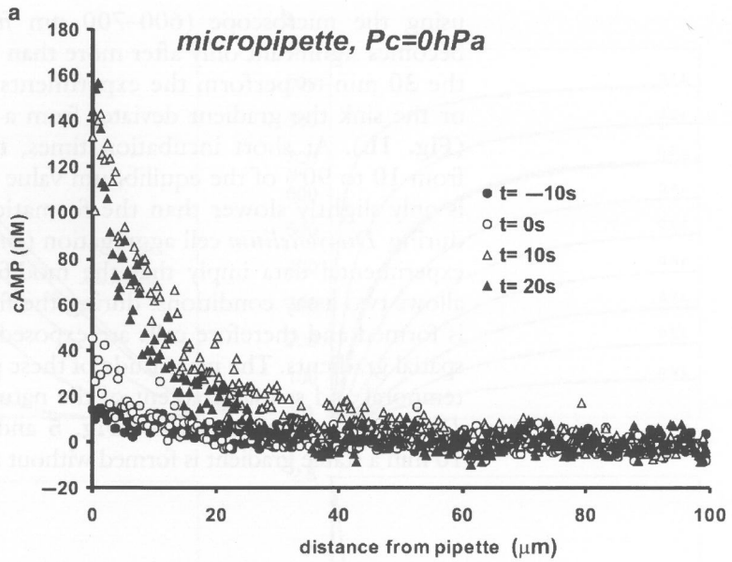

Fig. 3. Observed gradients in the micropipette assay. A micropipette filled with 100 μM cAMP and lucifer yellow was applied just above the glass surface in a droplet of cells. The fluorescence intensity was measured by confocal microscopy at different times after positioning of the pipette in the fluid. Initially no pressure was applied to the pipette (**a**), and a pressure of 25 hPa was applied at 20 s (**b**). The concentration of cAMP was deduced using a dilution series of lucifer yellow added homogeneously to the bath.

pressure of 25 hPa **(Fig. 3c)**. Similar to the case without applied pressure, the concentration rapidly decreases with distance from the pipette, except close to the pipette (within 2 μm) where the concentration remains relatively uniform.

3.3. Diffusion Equations for Pipette Gradients Without Flow

When a pipette filled with cAMP is positioned just above the floor of a chamber, cAMP will diffuse effectively in a half-sphere. The point of the pipette is in the center of the sphere; the opening of the pipette with opening r_0 is regarded as a small sphere from which cAMP diffuses. The diffusion equation is then given in sphere coordinates by:

$$\frac{\partial C(x,t)}{\partial t} = D\frac{1}{x^2}\frac{\partial}{\partial x}x^2\frac{\partial}{\partial x}C(x,t) \qquad (6)$$

In this equation D (μm²/s) denotes the diffusion coefficient of cAMP, $C(x,t)$ denotes the concentration at time t (s), and distance x (μm) from the pipette. We assume that the gradient in the pipette builds up very fast. Hence, equilibrium in the small sphere at the tip of the pipette will be reached rapidly leading to a constant concentration C_s at the tip. Numerical analysis of diffusion in the pipette and the small sphere suggests that the time constant of this process is less than 1 s. In addition, measurements presented in **Fig. 3b** reveal that equilibrium at the tip is reached within 10 s. We use the boundary condition that the concentration at the edge of the bath, $x = R$ is constant and zero. The complete space-time solution is then given by:

$$C(x,t) = C_s\frac{r_0}{x}\frac{R-x}{R-r_0} - C_s\frac{r_0}{x}\sum_{n=1}^{\infty}2a_n^{-1}\sin\left(a_n\frac{x-r_0}{R-r_0}\right)e^{-\frac{t}{\tau_n}} \qquad (7)$$

where $a_n = \pi n$, the time constants $\tau_n = a_n^{-2}\tau_D$ and $\tau_D = (R-r_0)^2/D$.

A very good approximation for **Eq. 7** is:

$$C(x,t) = C_s\frac{r_0}{x}\mathrm{erfc}\left(\frac{1}{2}\frac{x-r_0}{\sqrt{Dt}}\right) \qquad (8)$$

The time needed to reach this equilibrium strongly depends on the distance from the pipette $\tau_D = (x-r_0)^2/D$; when t equals this time constant about half-maximal equilibrium is reached.

After some time the gradient reaches equilibrium. The equilibrium concentration profile is given by the first term of **Eq. 7**, which for a large bath ($R \to \infty$) and $x > r_0$ is given by:

$$C(x) = C_s\frac{r_0}{x} = \frac{\alpha C_p}{x} \qquad (9)$$

where C_p is the cAMP concentration in the pipette. The absolute spatial gradient and the relative spatial gradient are then given by:

$$\nabla C(x) = -C_s\frac{r_0}{x^2} = -\frac{\alpha C_p}{x^2} \qquad (10)$$

and

$$\frac{\nabla C(x)}{C(x)} = -\frac{1}{x} \tag{11}$$

The experimental equilibrium data (**Fig. 4a**) were fitted using **Eq. 9** showing that they are in close agreement with the calculated

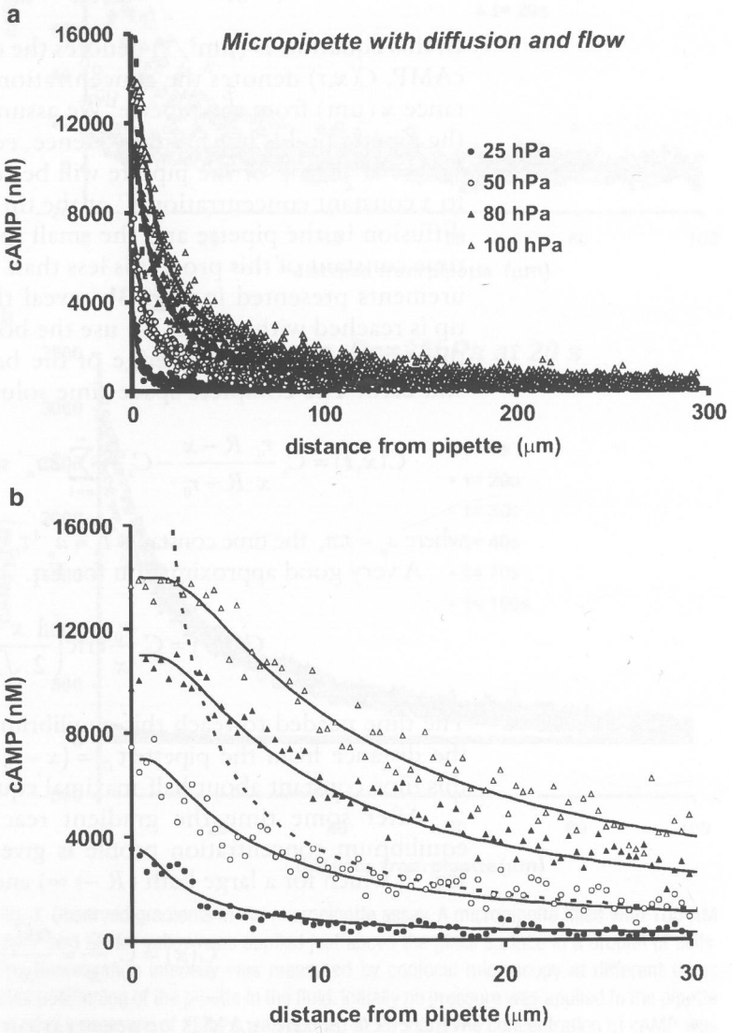

Fig. 4. Experimental equilibrium data of the cAMP gradient with different flow from the micropipettes. A micropipette filled with cAMP and lucifer yellow was applied just above the glass surface in a droplet of cells. The pressure applied was 25, 50, 80, and 100 hPa. The equilibrium fluorescence intensity was measured by confocal microscopy at 30 s after application of the pipette. The *lines* are the fitted data using **Eq. 13** with C_s and F as indicated in **Table 1**; the *dashed line* is **Eq. 17** for 50 hPa. The *lower panel* (**b**) shows the same data as *upper panel* (**a**), but only at shorter distance from the pipette.

gradient profile, except very close to the pipette. The experiment reveals that the measured cAMP concentration at the tip (i.e., C_s) is only 150 nM compared to 100 μM in the pipette, indicating that a very strong gradient is formed in the pipette.

3.4. Diffusion Equations for Pipette Gradients with Flow

When pressure is applied to the pipette, liquid will flow out of the pipette with flux F(μm³/s). To account for the flow the diffusion equation has to be extended with convection:

$$\frac{\partial C(x,t)}{\partial t} = D\frac{1}{x^2}\frac{\partial}{\partial x}x^2\frac{\partial}{\partial x}C(x,t) - \frac{F}{2\pi x^2}\frac{\partial}{\partial x}C(x,t) \tag{12}$$

A complete space-time solution of this equation is difficult to obtain. However, the equilibrium solution can be obtained relatively easy. For a large bath the steady-state concentration profile is given by:

$$C(x) = C_s\frac{1-e^{-\frac{F}{2\pi Dx}}}{1-e^{-\frac{F}{2\pi Dr_0}}} \tag{13}$$

The absolute spatial gradient and the relative gradient are then given by:

$$\nabla C(x) = -C_s\frac{F}{2\pi Dx^2}\frac{e^{\frac{F}{2\pi Dx}}}{1-e^{-\frac{F}{2\pi Dr_0}}} \tag{14}$$

and

$$\frac{\nabla C(x)}{C(x)} = -\frac{F}{2\pi Dx^2}\frac{e^{-\frac{F}{2\pi Dx}}}{1-e^{-\frac{F}{2\pi Dx}}} \tag{15}$$

The results shown in **Figs. 3** and **4** reveal that with an increase of pressure from 0 to 25 hPa, the concentration at the tip of the pipette increases substantially from 150 nM at 0 hPa to 3,000 nM at 25 hPa. In the absence of pressure, the concentration at the tip is very low due to limited diffusion in the narrow tip of the pipette, causing a large concentration gradient inside the pipette. With liquid flow, the liquid at the tip is replaced by interior liquid of higher concentration, resulting in a higher cAMP concentration at the tip.

The gradient profiles at different applied pressures (**Fig. 4**) were fitted using **Eq. 13**, yielding the values for the concentration at the tip (C_s) and flow (F) as presented in **Table 1**. The calculated lines are in very good agreement with experimental data, both close to the pipette and at longer distances from the pipette. This suggests that we derived and accurate model for gradient formation from a pipette with diffusion and flow.

Table 1
Values of *F* and C_s obtained by fitting experimental observations in Fig. 4 with Eq. 13

Applied pressure (P_c, hPa)	Fitted flow (F, μm³/s)	Fitted concentration at tip (C_s, nM)	$\alpha = \frac{C_s}{C_0}\frac{F}{2\pi D}$ (μ/m)
25	15.000	3,500	0.0875
50	30.000	7,000	0.35
80	48.000	11,000	0.88
100	60.000	14,000	1.4

Using the observed data and fitted values of F and C_s, **Eq. 13–15** can be simplified. The calculated flow is large relative to $2\pi Dr_0$, which implies that the denominator in **Eq. 13–15** reduces to 1. Furthermore, at longer distances from the pipette (i.e., at large x), $F/2\pi Dx$ in **Eq. 13** becomes very small, and consequently **Eq. 13** reduces to the following equation:

$$C(x) = C_s \frac{F}{2\pi Dx} \quad \text{(for large } x\text{)} \tag{16}$$

This equation has the same form as **Eq. 9**:

$$C(x) = \frac{\alpha C_p}{x} \tag{17}$$

where $\alpha = \frac{C_s}{C_p}\frac{F}{2\pi D}$ in $(\text{um})^{-1}$

In **Fig. 4** the dashed line represents **Eq. 17** with the experimentally fitted values of F and C_s, showing that the experimental data are very well described with the simple **Eq. 17** at distances beyond about 15 μm from the pipette. Finally, inspecting **Table 1**, we noted that the fitted values of both C_s and F increase linearly with the applied pressure P_c, indicating that α, and thus the absolute concentration, depends on P_c^2.

The usual field of observation is 100 × 100 μm with the pipette placed somewhere in the field. The time constant to reach equilibrium, $\tau_D = (x - r_0)^2 / D$, indicates that in the field of observation (x maximal 100 μm; $r_0 = 0.5$ μm, $D = 1{,}000$ μm²/s) equilibrium is reached within 10 s after application of the pipette, as was observed experimentally **(Fig. 3)**. Thus gradients from pipettes are essentially stable spatial gradients, except at very long distances from the pipette.

4. Gradients Generated by Aggregating *Dictyostelium* Cells

Dictyostelium cells secrete cAMP in a pulsatile manner with a periodicity of about 5 min. The cAMP signal is relayed through the field leading to waves of cAMP that propagate with a velocity of about 300 mm/min. These waves have been visualized by fluorography using competition between secreted cAMP and added [³H]cAMP for binding to a cAMP-binding protein.

We calculated the extracellular cAMP concentration during natural cell aggregation using the original fluorographs made by Tomchik and Devreotes *(12)* as presented in *(13)*. The fluorographs represent the competition of a fixed amount of [³H]cAMP and secreted cAMP for binding to the regulatory subunit of cAMP-dependent protein kinase. In essence, this experiment is an isotope dilution assay in space that follows the equation:

$$A(x) = a\left[\frac{C_0 - bl}{C_x - bl} - 1\right] \tag{18}$$

where $A(x)$ is the cAMP concentration at position x, C_0 is the amount of [³H]cAMP-binding in the absence of cAMP, bl is the blanc of the assay (i.e., the amount of [³H]cAMP-binding in the presence of excess cAMP), C_x is the amount [³H]cAMP-binding at position x competed by unknown amount of cAMP, and a is a proportionality constant that is determined by measuring the amount [³H]cAMP-binding at known amounts of unlabelled cAMP. For cAMP determinations in a test tube, the measured units are counts per minute (cpm), while in fluorographs the units are in gray scales. We determined the proportionality constant a in a test tube (550 nM), and estimated the values of C_0 and bl from the information provided by Devreotes et al. *(13)*. C_0 is the gray level in the absence of cAMP (127 in **Fig. 2** from **ref.** *13)*, while bl is the gray level in the presence of saturating cAMP (90 in **Fig. 2** from **ref.** *13)*. The cAMP concentration in natural waves was calculated as the average of two successive waves. From the spatial resolution and the speed of wave propagation we calculated the spatial cAMP gradient and the temporal cAMP gradient during cell aggregation.

The results **(Fig. 5)** show that the extracellular cAMP concentration profiles are approximately symmetric cAMP waves. The width at the base of the wave is about 1,600 μm. Since the wave travels at a speed of about 300 μm/min, the periodicity of the wave is approximately 5–6 min. The rising flank of the wave, as well as the width at half-maximal concentration, is about 450 μm or 1.5 min. The absolute spatial gradient of the wave, $\nabla C = dC/dx$, increases during the rising flank of the wave and reaches a maximum of about 4 nM/μm at about 1 min after arrival

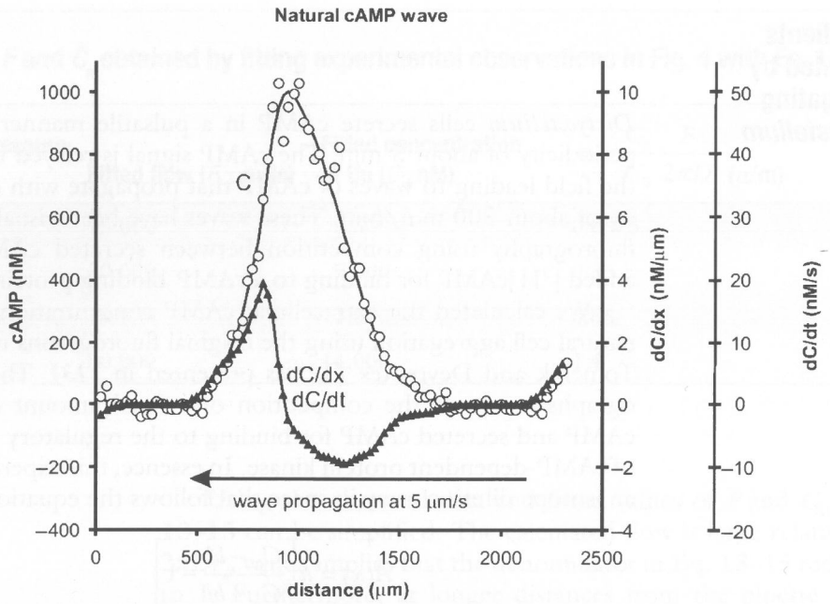

Fig. 5. Natural cAMP wave during cAMP aggregation. The cAMP concentration was deduced from fluorographs of released cAMP measured by ***(13)***. For calculations *see* part 4. Gradients Generated by Aggregating *Dictyostelium* Cells the wave of CAMP travels through a filed of cells at a rate of about 300 μm/min (5 μm/s).

of the cAMP wave. This absolute spatial gradient is only twofold larger than the maximal spatial gradient in the Zigmond chamber of 1.8 nM/μm (*see* **Fig. 5**). The relative steepness of the wave, $\nabla C/C$ is around 0.007 $(um)^{-1}$ during most of the rising flank of the cAMP wave (i.e., 7% concentration difference between front and back of a 10-mm long cell).

The cAMP waves are propagated in the field of cells with a speed $v = dx/dt$ of 300 μm/min ***(13)***. Therefore, the temporal gradient is given by $dC/dt = v\nabla C$ Thus, the temporal gradient follows the spatial gradient and reaches a maximum value of about 17.5 nM/s at 1-min after arrival of the cAMP wave. In the Zigmond chamber the temporal gradient reaches a maximum of 3 nM/s at 2 min after application of cAMP **(Fig. 1c)**.

5. Conclusions

The gradients formed in the modified Zigmond assay are very different from the gradients formed by a point source releasing a constant flux of cAMP. The major differences are: a temporal-spatial

gradient with little distance dependency in the Zigmond assay versus a stable gradient with very strong distance dependency. It is surprising that the distance dependency of the pipette assay is often not taken into account, exemplified by the absence of information on the distance from the pipette where the chemotaxis data were obtained, a situation we also were not aware of in the past ***(14)***. Chemotaxis in *Dictyostelium* is mainly dependent on the absolute spatial gradient resulting in only about 10 occupied receptors more at the front of the cells relative to the rear of the cell at threshold conditions, at prevailing receptor occupancies of around 1,000 receptors. It will be a major effort to uncover how cells are able to deduce spatial information from a signal that is inherently very noisy due to the high average receptor occupancy. The gradient models presented here may help to design experiments to deduce the fundamental principles of gradient sensing and directed locomotion.

Acknowledgments

We thank Douwe Veltman and Ineke Keizer-Gunnink for obtaining experimental data on the Zigmond chamber **(Fig. 1)** and micropipettes **(Figs. 3** and **4)**, respectively.

References

1. Szurmant, H. and Ordal, G. W. (2004) Diversity in chemotaxis mechanisms among the bacteria and archaea. *Microbiol. Mol. Biol. Rev.* **68**, 301–319.
2. Devreotes, P. and Janetopoulos, C. (2003) Eukaryotic chemotaxis: distinctions between directional sensing and polarization. *J. Biol. Chem.* **278**, 20445–20448.
3. Servant, G., Weiner, O. D., Herzmark, P., Balla, T., Sedat, J. W., and Bourne, H. R. (2000) Polarization of chemoattractant receptor signaling during neutrophil chemotaxis. *Science.* **287**, 1037–1040.
4. Affolter, M. and Weijer, C. J. (2005) Signaling to cytoskeletal dynamics during chemotaxis. *Dev. Cell.* **9**, 19–34.
5. Parent, C. A. and Devreotes, P. N. (1999) A cell's sense of direction. *Science.* **284**, 765–770.
6. Van Haastert, P. J. M. and Devreotes, P. N. (2004) Chemotaxis: signalling the way forward. *Nat. Rev. Mol. Cell. Biol.* **5**, 626–634.
7. Futrelle, R. P. (1982) *Dictyostelium* chemotactic response to spatial and temporal gradients. Theories of the limits of chemotactic sensitivity and of pseudochemotaxis. *J. Cell. Biochem.* **18**, 197–212.
8. Iijima, M., Huang, Y. E., and Devreotes, P. (2002) Temporal and spatial regulation of chemotaxis. *Dev. Cell.* **3**, 469–478.
9. Varnum-Finney, B., Edwards, K. B., Voss, E., and Soll, D. R. (1987) Amoebae of *Dictyostelium discoideum* respond to an increasing temporal gradient of the chemoattractant cAMP with a reduced frequency of turning: evidence for a temporal mechanism in ameboid chemotaxis. *Cell Motil. Cytoskeleton.* **8**, 7–17.
10. Veltman, D. M. and Van Haastert, P. J. (2006) Guanylyl cyclase protein and cGMP product independently control front and back of chemotaxing *Dictyostelium* cells. *Mol. Biol. Cell.* **17**, 3921–3929.
11. Swanson, J. A. and Taylor, D. L. (1982) Local and spatially coordinated movements in *Dictyostelium discoideum* amoebae during chemotaxis. *Cell.* **28**, 225–232.
12. Tomchik, K. J. and Devreotes, P. N. (1981) Adenosine 3′,5′-monophosphate waves in

Dictyostelium discoideum: a demonstration by isotope dilution-fluorography. *Science.* **212**, 443–446.

13. Devreotes, P. N., Potel, M. J., and MacKay, S. A. (1983) Quantitative analysis of cyclic AMP waves mediating aggregation in *Dictyostelium discoideum*. *Dev. Biol.* **96**, 405–415.
14. Loovers, H. M., Postma, M., Keizer-Gunnink, I., Huang, Y. E., Devreotes, P. N., and van Haastert, P. J. (2006) Distinct roles of PI(3,4,5)P_3 during chemoattractant signaling in *Dictyostelium*: a quantitative in vivo analysis by inhibition of PI3-kinase. *Mol. Biol. Cell.* **17**, 1503–1513.

Chapter 32

Modeling Spatial and Temporal Dynamics of Chemotactic Networks

Liu Yang and Pablo A. Iglesias

Summary

When stimulated by chemoattractants, eukaryotic cells respond through a combination of temporal and spatial dynamics. These responses come about because of the interaction of a large number of signaling components. The complexity of these systems makes it hard to understand without a means of systematically generating and testing hypotheses. Computer simulations have proved to be useful in testing conceptual models. Here we outline the steps required to develop these models.

Key words: Mathematical model, Chemotaxis, Reaction–diffusion, Systems biology, Virtual cell

1. Introduction

What does a mathematical model tell me that I didn't know before? This is a common question posed by experimenters, suspicious that models merely package already-known information and provide few new insights. Models can do two things. First, they can "verify that known interactions in some system can produce the observed qualitative behavior" *(1)*. When employed this way, models act mostly as tools providing a form of consistency check, ensuring that the posited conceptual models behave as they are supposed to. However, the real benefit of models is a predictive tool. In this case, models usually precede complete knowledge of the system but serve to channel experimental investigations.

It is usually thought that the introduction of mathematical and computational techniques in the study of signaling pathways is a relatively new phenomenon – an offshoot of the

Tian Jin and Dale Hereld (eds.), *Chemotaxis,* Methods in Molecular Biology, vol. 571
DOI 10.1007/978-1-60761-198-1_32,